Short communication

Fabrication of Te@Au core-shell hybrids for efficient ethanol oxidation

Huile Jin [a], Demeng Wang [a], Yuewu Zhao [a], Huan Zhou [a], Shun Wang [a,*], Jichang Wang [b,**]

[a] Nano-materials & Chemistry Key Laboratory, Wenzhou University, Wenzhou, Zhejiang 325035, China
[b] Department of Chemistry and Biochemistry, University of Windsor, ON, Canada N9B 3P4

HIGHLIGHTS

► A simple template/reduction approach is developed for fabricating Te@Au hybrids.
► The Te@Au hybrid electrode exhibits much higher electrocatalytic activity in ethanol oxidation.
► The hybrids have higher tolerance on the poisoning by intermediate products.
► The effective surface area was greatly increased due to the formation of Au nanoparticles.

ARTICLE INFO

ABSTRACT

Using Au nanoparticles to catalyze the oxidation of alcohols has garnered increasing attention due to its potential application in direct alcohol fuel cells. In this research Te@Au core-shell hybrids were fabricated for the catalytic oxidation of ethanol, where the preparation procedure involved the initial production of Te crystals with different microstructures and the subsequent utilization of the Te crystal as a template and reducing agent for the production of Te@Au hybrids. The as-prepared core-shell hybrids were characterized by scanning electron microscopy, transmission electron microscopy, energy-dispersive X-ray spectroscopy, and X-ray diffraction techniques. Electrochemical measurements illustrate that the hybrids have great electrocatalytic activity and stability toward ethanol oxidation in alkaline media. The enhanced electrocatalytic property may be attributed to the cooperative effects between the metal and semiconductor and the presence of a large number of active sites on the hybrids surface.

© 2012 Elsevier B.V. All rights reserved.

1. Introduction

Micro/nano materials with a three-dimensional (3D) superstructure have shown interesting mechanical, electrical and electromagnetic properties [1–5], and have been used in electronics, optics, optoelectronics, electrochemical sensors and chemical catalysis [6,7]. Among those 3D nanostructured materials reported, the p-type semiconductors with a narrow-band gap such as trigonal tellurium (Te) have demonstrated particularly promising properties such as great photoconductivity and catalytic activity [8]. Te has also served as a sacrificial template to synthesize other nanomaterials with a desired morphology, making the development of simple and inexpensive methods for controllable synthesis of Te a rather important topic [9]. Significant progresses in the synthesis of one- and three-dimensional Te nanomaterials such as rods [8], wires [9–11], tubes [12], spheres, flowers [13] and dendrites [14] have been achieved in the past decade. Zhu and co-workers, for example, synthesized Te nanotubes, nanowires and nanorods on a large scale through the reduction reaction of K_2TeO_3 and NaH_2PO_2, in which the morphology was tuned by controlling NaOH concentration, reaction temperature and reductant concentration [8].

A facile route for fabricating semiconductor nanocables using Te nanowire as the core and carbon as shell (Te@C) has been developed by Wang and co-workers [10]. Their experiments demonstrated that the shell thickness of the Te@C nanocables could be easily tuned by controlling the deposition time and the concentration of dextran. Xia and co-workers studied the chemical transformation of various ultrathin metal telluride nanowires (i.e. M_xTe_y with M = Ag, Cd, Zn, Pb, or Pt), where ultrathin Te nanowires were converted into Ag_2Te nanowires through topotactic transformation. Later, the Ag_2Te nanowires were transformed into CdTe, ZnTe, and PbTe nanowires through cation exchange [3]. The feasibility of using Te as a template to make other nanomaterials has significantly expanded its application in areas such as catalysis.

* Corresponding author. Tel.: +86 577 86689357; fax: +86 577 86689300.
** Corresponding author. Fax: +1 519 973 7098.
   E-mail addresses: shunwang@wzu.edu.cn (S. Wang), jwang@uwindsor.ca (J. Wang).

The use of Au to facilitate the oxidation of simple alcohols has recently garnered a great deal of attention [15–17]. When Au nanoparticles were used to form composites, such as Au on reducible metal oxides, stronger catalytic activity was achieved in prompting the oxidation of CO and alkenes at low temperature [18,19]. This is consistent with a number of reports that demonstrated the so-called cooperative effects when metal nanoparticles are dispersed on the semiconductor surface [20–22]. In this research we explored the feasibility of utilizing Te dendrites as a template and reducing agent to synthesize Te@Au core-shell hybrids. In comparison to methods developed earlier for the preparation of Au composites, the current approach only requires to prefabricate Te crystals with a desired morphology, not both components with a desired microstructure. In addition, the techniques of making 3D Te crystals have been well established [8–15]. The template/reducing agent approach also puts a growth limit (i.e. the thickness) of the shell layer, which consequently reduces the need of precious metals. The thin film property may further amplify the cooperative interaction of the metal and semiconductor.

2. Experimental

2.1. The synthesis of Te@Au hybrids

$HAuCl_4 \cdot 4H_2O$, KOH, ethylene glycol, acetone, hydrazine (50%) and ethanol were purchased from Shanghai Chemical Factory, China and were used as received. Nafion (perfluorinated ion-exchange resin, 5 wt% solution in a mixture of lower aliphatic alcohols and water) was obtained from Aldrich. Deionized water used in this study was prepared with a Millipore system. The dendrite-shaped Te crystals were prepared according to our prior work [13]. The large scale synthesis of Te@Au hybrids was carried out through the following strategy: 18.6 mg of Te dendrites was added into 20.0 mL of ethylene glycol, followed by the addition of 4.0 mL of 10.0 mM $HAuCl_4$ solution. The mixture was stirred at 50 °C until the Au precursor was reduced completely, which took about 2 h. The solution was then centrifuged and the collected solid was washed several times with deionized water and absolute ethanol. Finally, the product was dried at 70 °C in vacuum condition for 12 h.

2.2. Preparation of the working electrodes

Prior to the surface coating, glass carbon (GC) electrodes were polished carefully with 1.0, 0.3 and 0.05 μm alumina powder, respectively, and rinsed with deionized water. It was followed by sonication in acetone and deionized water. The cleaned GC electrode was then dried with nitrogen gas. About 5.0 mg of Te@Au hybrids was ultrasonically suspended in a mixture of 2.0 mL of ethanol and 50.0 uL of 5 wt % Nafion solution for about 30 min to obtain an ink. 20.0 μL of the catalyst ink was then spread on the surface of a GC electrode (area = 0.124 cm^2).

When polycrystalline Au electrode was investigated, a1.5 mm diameter Au electrode (CH Instruments, Chenhua Co., China) was first polished with 0.3 μm alumina slurry on a polishing cloth for approximately 5 min. After that the electrode was rinsed with water and then cleaned ultrasonically in deionized water for 1 min to remove residual alumina particles that might have been trapped on the surface. Electrochemical pretreatment was performed with 25 successive scans between −0.2 V and 1.1 V (vs. Ag/AgCl) in a 0.5 M H_2SO_4 solution at a scan rate 100 mV s^{-1}. After that, the electrode was rinsed with water and then ultrasonicated in water for 1 min [23,24]. The effective surface area (ESA) of the working electrodes was determined with cyclic voltammetry (CV) technique. The scan took place in a 1.0 M KOH solution. Integration of the charge consumed during the formation of the surface oxide

monolayer enabled the estimation of ESA using a reported reference value of 386 μC cm^{-2} [23,24].

2.3. Characterization and electrochemical measurements

A FEI Nova Nanosem 200 scanning electron microscope (SEM) was used to determine the morphology and compositions of the Te@Au products. Transmission electron microscopy (TEM) measurements were made on a JEOL 2100F microscope with a 200 kV accelerating voltage (Japanese Electron Optics Laboratory). X-ray diffraction (XRD) pattern was recorded with a Bruker D8 Advance X-ray diffractometer using Cu Kα radiation with a Ni filter. The 2θ angular regions between 20° and 80° were explored at a scan rate of 5° min^{-1}. Cyclic voltammetry experiments were performed with a CHI660c electrochemical analyzer (CH Instruments, Chenhua Co., China), where a conventional three-electrode cell was used with Ag/AgCl (saturated KCl) as the reference electrode, a platinum wire as the counter electrode and Te@Au modified GC as the working electrode.

3. Results and discussion

Fig. 1 shows SEM images of the as-obtained Te (panels (a) and (b)) and Te@Au hybrids (panels (c) and (d)). Fig. 1(a) illustrates that these Te crystals have a dendrite shape. From the magnified SEM image in Fig. 1(b), it can be seen that these Te dendrites have a length of up to 30 μm and the diameter of those secondary branches ranges between 75 and 150 nm. Comparison of Fig. 1(b) and (d) leads to a conclusion that the dendrite framework is not destroyed upon the reduction reaction between Te and Au^{3+} ions.

Fig. 2(a) is a TEM image taken at the tip of a Te@Au dendrite. From this image, it is clear that the Te dendrites are covered by Au film and, interestingly, the film is not smooth and consists of Au nanospheres. The presence of Au nanoparticles on the surface is expected to significantly increase the surface area and the number of active sites, which shall have positive impacts on the catalytic activity. Fig. 2(b) is a HRTEM image, which shows that the d-spacing is 0.235 nm. Such a fringe spacing agrees well with the spacing of Au (111) plane [25]. This conclusion is further confirmed by XRD spectra. HRTEM image in Fig. 2(b) also illustrates that Au atoms are well-distributed on the Te surface, forming an enclosed shell. A high angle annular dark field (HAADF) image of the secondary branch is shown in Fig. 3(a), where the core-shell structure can be easily recognized. The Te core is a bright spot at the center and the outer shell is designated Au. Variation of the HAADF contrast can be attributed to the thickness change. This image also shows that the Au film is not smooth, where Au particles with a size between 3 and 10 nm can be identified. Our experiments illustrate that the roughness of the Au film (i.e. the size of these Au NPs) are influenced by the initial concentration of Au^{3+}. The element distribution across the secondary branch is analyzed by the line scanning analysis in the STEM EDS mode. The result, presented in Fig. 3(b), reveals that Te concentration peaks at the core, whereas Au element peaks near the edge of the branch. Overall, the above characterization shows that Au distributes all over the dendrites, whereas Te is negligible on the exterior of the hybrids.

Fig. 4 shows the XRD spectra of (a) Te crystal and (b) Te@Au hybrids. All the diffraction peaks in the Te pattern can be readily indexed to the hexagonal Te with the calculated lattice parameters in good agreements with literature values (JCPDS 34-0420). For the Te@Au hybrids, four peaks corresponding to the (111), (200), (220), and (311) planes of a face-centered cubic lattice of Au have been observed (JCPDS No. 04-0784). The peak corresponding to the (111) plane is more intense than peaks corresponding to the other planes. This confirms that Te@Au core-shell hybrids have been successfully
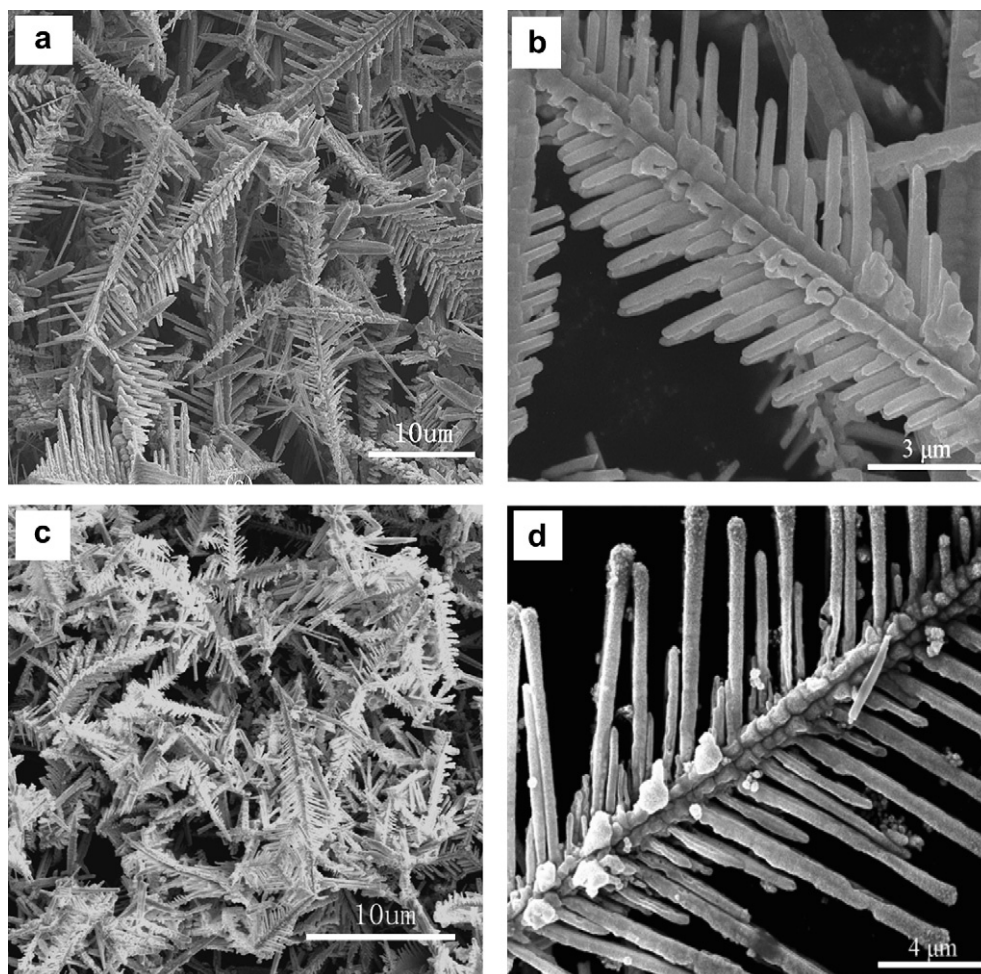
Fig. 1. SEM images of (a and b) Te and (c and d)Te@Au hybrids.

synthesized by the template-reduction route, where the Au film grew along (111) direction.

Fig. 5(a) shows CVs at the polycrystalline Au and the Te@Au hybrid electrodes in a 1.0 M KOH solution. For the Au electrode, a broad oxidation wave in the potential range between 30 and 400 mV and a reduction peak at −100 mV were observed, which correspond respectively to the formation and reduction of surface oxides. This is atypical behavior of Au in alkaline electrolyte [26]. The voltammogram of Te@Au electrode is largely the same as that of the poly-Au electrode,the stronger peak current can be
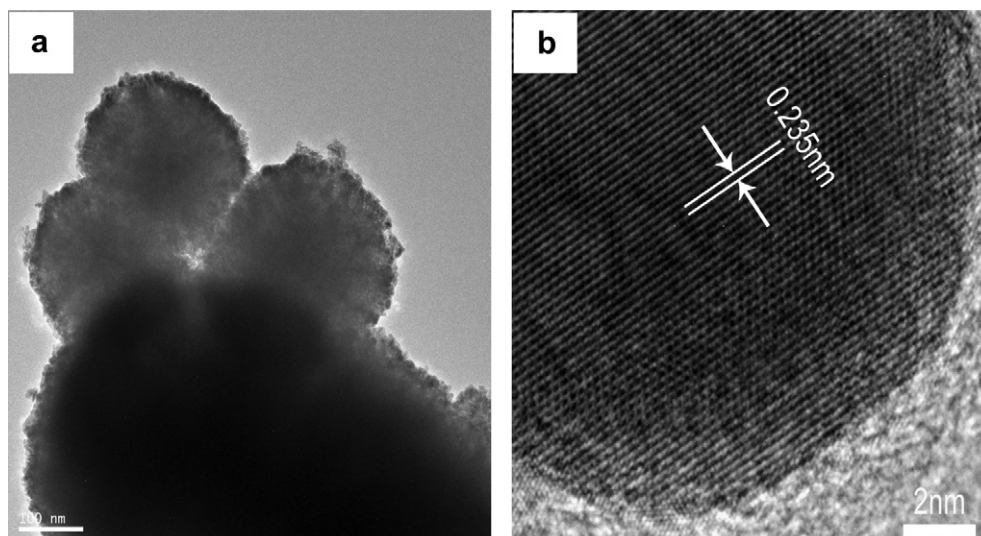

Fig. 2. (a) TEM and (b) HRTEM images recorded at the tip of Te@Au hybrids.
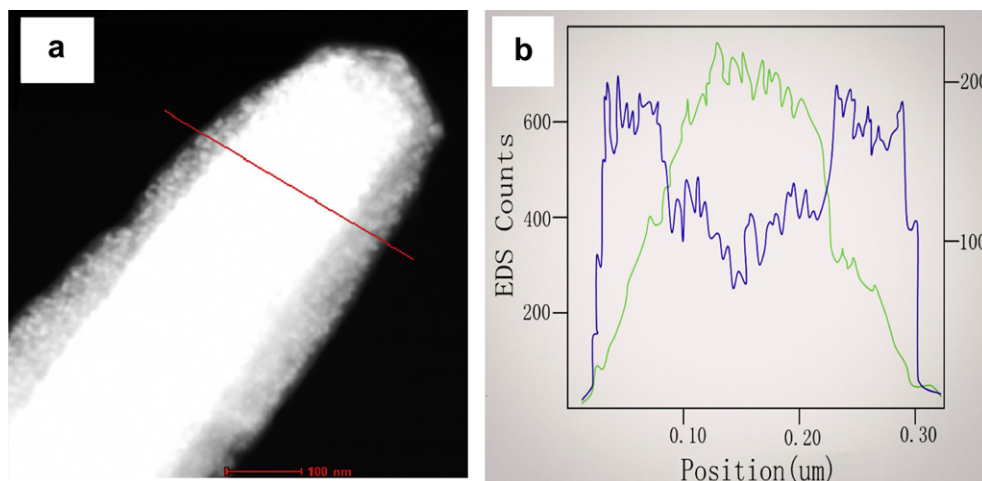
Fig. 3. (a) HAADF image measured at the tip of Te@Au hybrids. (b) Characterization of Te and Au distribution across a secondary branch of the dendrite. EDS line profile of Te (green) and Au (blue) through the area indicated by the red line in (a). (For interpretation of the references to colour in this figure legend, the reader is referred to the web version of this article.)

attributed to the significant increase in the surface area. The effective surface area of both working electrodes can be estimated from the amount of charge consumed during the reduction of the surface Au oxide monolayer divided by a reported parameter value of 386 $\mu C\ cm^{-2}$. The ESA of the poly-Au and Te@Au hybrids electrodes are measured to be 0.235 and 1.174 cm^2, respectively. The total electrochemical active surfaceareas (ECSAs)of Te@Au hybrids is therefore 458% of the poly-Au electrode. The significant increase in ECSA indicates that the as-prepared Te@Au core-shell dendrites could be potentially used as an efficient electrocatalyst.

CVs of 1.0 M ethanol in a 1.0 M KOH solution measured with poly-Au and Te@Au hybrids electrodes are shown in Fig. 5(b), where the scanning rate was 50.0 mV s^{-1}.The anodic peak potentials are 310 and 200 mV for the Te@Au and poly-Au catalyst electrode, respectively. With the Te@Au hybrids electrode there is approximately 100 mV positive shift in the anodic peak potential, but a much higher CH$_3$CH$_2$OH oxidation current density is obtained. Specifically, the peak current densities are 11.58 and 2.24 mA cm^{-2} at the Te@Au and poly-Au electrodes, respectively. The current density was calculated on the basis of ECSA that was determined above. Although the anodic peak potential shifted positively, the oxidation onset potential at Te@Au electrode became −0.30 V, which was lower than −0.20 V obtained with poly-Au catalyst. The semiconductor Te did not reduce the

conductivity of the hybrids, which is presumably because high density Au NPs had formed the necessary electric network on the hybrids surface [27]. In comparison to the spectra in Fig. 5(a), the cathodic peak in Fig. 5(b) is significantly reduced, implicating that a smaller amount of Au oxides was produced during the forward scan in the ethanol solution. It provides further support that Au has catalytic effect on the electro-oxidation of ethanol, since it reduces the quantity of Au oxides on the electrode surface.

Anodic peaks associated with ethanol oxidation are observed in both the forward and reverse sweeps. The oxidation peak observed in the reverse scan is primarily associated with the removal of the adsorbed intermediate products formed during the forward scan. The ratio of the forward and reversed oxidation current peaks, I_f/I_b, is an important measure of the tolerance of the catalyst to fouling [28–30]. A higher ratio indicates the better tolerance against the poisoning species. Recently, several reports have demonstrated that Au@Pt and Au@Pd core/shell hybrids or their alloy NPs have higher electrocatalytic activity than Pt (or Pd) NPs. They also exhibited particular advantage in effectively removing the poisoning species through a bifunctional mechanism [31–34]. For the Te@Au hybrids electrode, Fig. 5(b) shows that the anodic peak during the reverse scan has almost disappeared, indicating that it has very high tolerance on poisoning. The improved tolerance on carbon intermediate products may be attributed to that reducible gold oxides
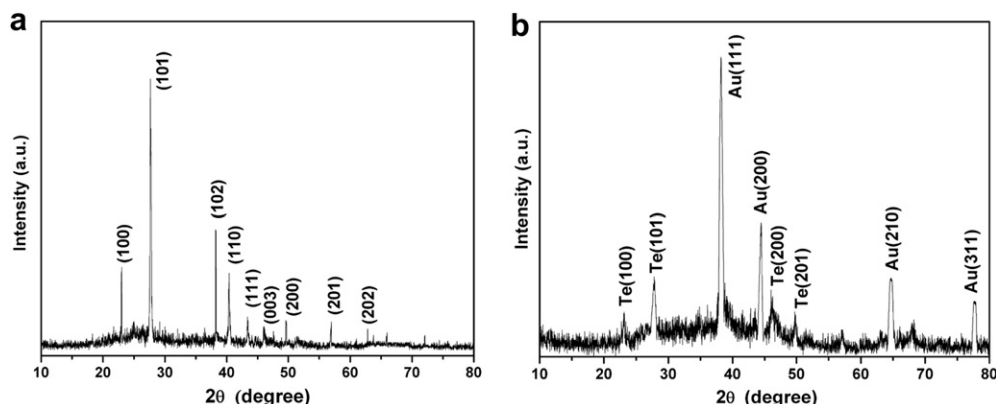

Fig. 4. XRD patterns of (a)Te and (b)Te@Au hybrids.
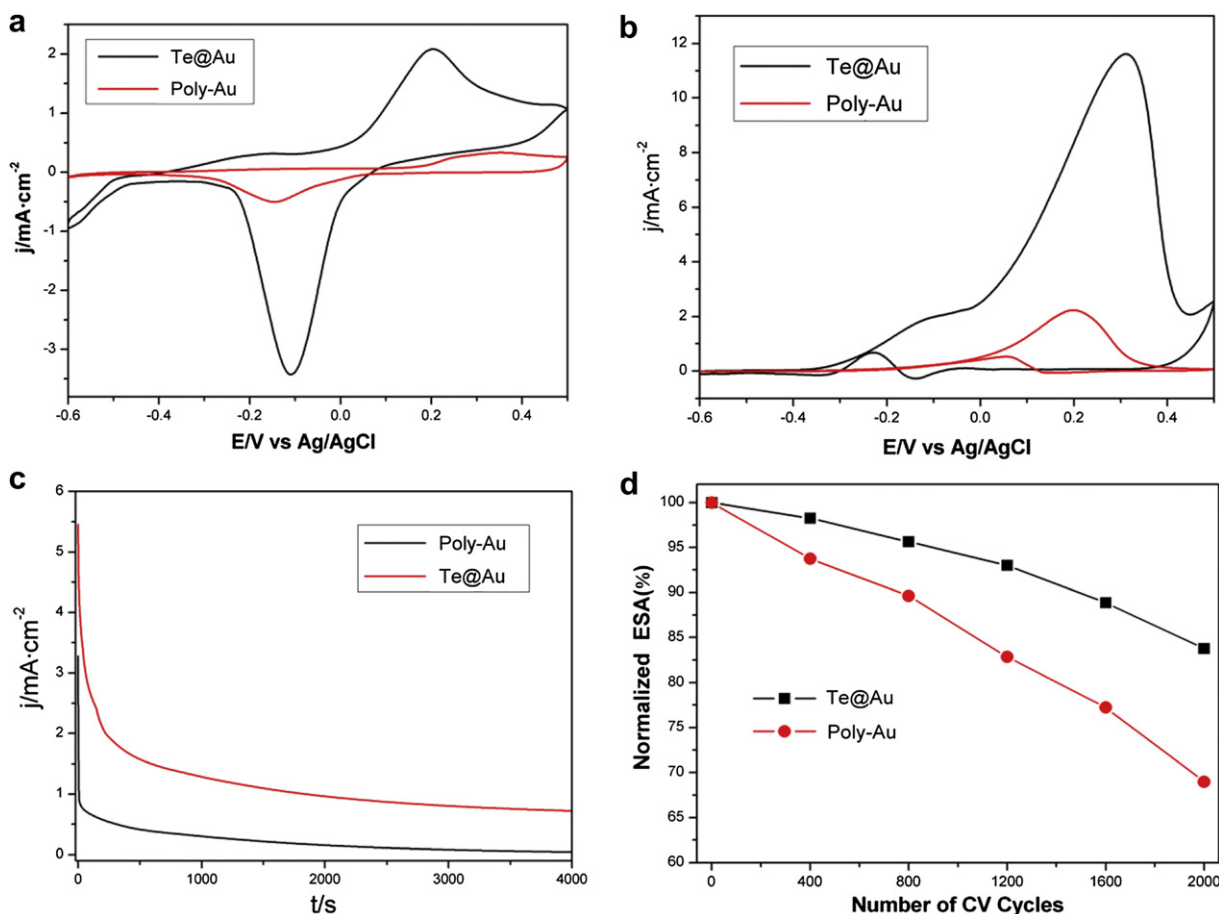
Fig. 5. CVs at poly-Au and Te@Au electrodes in (a) 1.0 M KOH and (b) 1.0 M KOH + 1.0 M ethanol solution; (c) Chronoamperometric curves for the poly-Au and Te@Au electrodes in 1.0 M KOH and 1.0 M ethanol solution; (d) Normalized ECSA of the poly-Au and Te@Au electrodes as a function of the cycling numbers in the accelerated durability tests. The scan rate in (a) and (b) is 50 mV s^{-1}.

promote the oxidation of intermediate products such as CO at low temperature.

The stability of the Te@Au hybrids electrode was investigated by chronoamperometric experiments at 100 mV (versus Ag/AgCl). From Fig. 5(c), one can see that the current decay of the hybrids is much slower than that of poly-Au. At 4000 s, for example, the current is 0.73 mA cm^{-2} at the Te@Au electrode, whereas it is only 0.043 mA cm^{-2} at the poly-Au electrode. The current decay is generally associated with the poisoning by ethanol oxidation products. Therefore, results in Fig. 5(c) suggest that Te@Au hybrids does not only enhance the catalytic activity of Au, but also produces better electrocatalytic stability toward poisoning [31,32,35]. In Fig. 5(d), the accelerated durability tests of the electrodes were conducted by potential cycling in a O$_2$-purged 1.0 M KOH solution at room temperature with a scan rate of 50 mV s^{-1}. After 4000 cycles, the poly-Au catalyst had lost 31% of its initial ECSA, while the degradation of Te@Au hybrids is less serious, with 17.2% loss of its activity.

4. Conclusions

Te crystals with a dendrite microstructure were prepared and utilized as a template and reducing agent to prepare Te@Au core-shell hybrids. Characterizations with SEM and TEM illustrate that the coating of Te crystal by Au film does not destroy the morphology. Considering that no surfactant or external template is needed, the method developed in this study represents a simple

and green approach for fabricating Au composites. This template-reduction approach can in principle be expanded to the preparation of other semiconductor/metal composites. Notably, using the core as a reducing agent also ensures that the coating layer is thin and thus reduces the usage of precious metals such as Au. The enhanced electrocatalytic property toward ethanol oxidation may be attributed to the combination of the cooperative effect between metal and semiconductor and the presence of a large number of active sites on the surface that facilitate the adsorption of active oxygen atoms and thus the oxidation of intermediates adsorbed on the catalysts [36]. The improved electrocatalytic activity and higher tolerance on fouling indicate that Te@Au hybrids is a good candidate in constructing ethanol-based fuel cells.

Acknowledgments

References

[1] D.G. Bell, L.X. Dong, B.J. Nelson, Nano Lett. 6 (2006) 725–729.
[2] H. Ogihara, M. Sadakane, Y. Nodasaka, W. Ueda, Chem. Mater. 18 (2006) 4981–4983.
[3] G.D. Moon, S. Ko, Y. Xia, U. Jeong, ACS Nano 4 (2010) 2307–2319.
[4] N. Tang, W. Zhong, C. Au, Y. Yang, M. Han, K. Lin, Y. Du, J. Phys. Chem. C 112 (2008) 19316–19323.
[5] X.Y. Kong, Z.L. Wang, Nano Lett. 3 (2003) 1625–1631.

[6] H. X.Yu, J.K. Zhang, P.V. Oliverrio, Bravn. Nano Lett. 9 (2009) 4424–4427.
[7] Y. Li, W. Cai, G. Duan, Chem. Mater. 20 (2008) 615–624.
[8] H. Zhu, H. Zhang, J. Liang, G. Rao, J. Li, G. Liu, Z. Du, H. Fan, J. Luo, J. Phys. Chem. C 115 (2011) 6375–6380.
[9] W. Lu, Y. Ding, Y. Chen, Z.L. Wang, J. Fang, J. Am. Chem. Soc. 127 (2005) 10112–10116.
[10] W. Wang, L. Sun, Z. Fang, L. Chen, Z. Zhang, Cryst. Growth Des. 9 (2009) 2117–2123.
[11] H. Qian, E. Zhu, S. Zheng, Z. Li, Y. Hu, C. Guo, X. Yang, L. Li, G. Tong, H. Guo, Nanotechnology 21 (2010) 495602–495607.
[12] H. Fan, Y. Zhang, M. Zhang, X. Wang, Y. Qian, Cryst. Growth Des. 8 (2008) 2838–2841.
[13] S. Wang, W. Guan, D. Ma, X. Chen, L. Wan, S. Huang, J. Wang, CrystEngComm. 12 (2010) 166–171.
[14] S. Wang, K. Zhang, H. Zhou, W. Guan, D. Ma, J. Lin, L. Zhang, S. Huang, J. Wang, CrystEngComm. 12 (2010) 3852–3857.
[15] Y. Cai, M. Zhou, M. Zeng, C. Zhang, Y.P. Feng, Nanotechnology 22 (2011) 215702–215707.
[16] J. Zhang, P. Liu, H. Ma, Y. Ding, J. Phys. Chem. C 111 (2007) 10382–10388.
[17] D.A. McCurry, M. Kamundi, M. Fayette, F. Wafula, N. Dimitrov, ACS Appl. Mater. Interfaces 3 (2011) 4459–4468.
[18] J. Gong, C.B. Mullins, J. Am. Chem. Soc. 130 (2008) 16458–16459.
[19] M. Haruta, T. Kobayashi, H. Sano, N. Yamada, Chem. Lett. 16 (1987) 405–408.
[20] C.C. Jia, H.M. Yin, H.Y. Ma, R.Y. Wang, X.B. Ge, A.Q. Zhou, X.H. Xu, Y. Ding, J. Phys. Chem. C 113 (2009) 16138–16143.
[21] M.S. Chen, D.W. Goodman, Science 306 (2004) 252–255.
[22] J.A. Rodriguez, S. Ma, P. Liu, J. Hrbek, J. Evans, M. Perez, Science 318 (2007) 1757–1760.
[23] H. Zhang, J.J. Xu, H.Y. Chen, J. Phy. Chem. C 112 (2008) 13886–13892.
[24] R.F. Carvalha, R.S. Freire, L.T. Kubota, Electroanalysis 17 (2005) 1251–1259.
[25] W. Li, H. Ma, J. Zhang, X. Liu, X. Feng, J. Phys. Chem. C 113 (2009) 1738–1745.
[26] Z. Borkowska, A. Tymosiak-Zielinska, G. Shul, Electrochim. Acta 49 (2004) 1209–1220.
[27] S. Guo, S. Dong, E. Wang, J. Phys. Chem. C 114 (2010) 4797–4802.
[28] F. Ksar, L. Ramos, B. Keita, L. Nadjo, P. Beaunier, H. Remita, Chem. Mater. 21 (2009) 3677–3683.
[29] M.D. Obradovic, J.R. Rogan, B.M. Babic, A.V. Tripkovic, J. Power Source 197 (2012) 72–79.
[30] Y.W. Lee, M. Kim, S.W. Kang, J.H. Lee, S.W. Han, J. Phys. Chem. C 114 (2010) 7689–7693.
[31] Q.G. He, W. Chen, S. mukerjee, J. Power Sources 187 (2009) 298–304.
[32] T. Maiyalagan, K. Scott, J. Power Source 195 (2010) 5246–5251.
[33] J. Liu, L. Cao, W. Huang, Z. Li, ACS Appl. Mater. Interfaces 3 (2011) 3552–3558.
[34] L. Zhang, J. Zhang, Q. Kuang, S. Xie, Z. Jiang, Z. Xie, L. Zheng, J. Am. Chem. Soc. 133 (2011) 17114–17117.
[35] X. Teng, Q. Wang, P. Liu, W. Han, A.I. Frenkel, W. Wen, N. Marinkovic, J.C. Hanson, J.A. Rodriguez, J. Am. Chem. Soc. 130 (2008) 1093–1101.
[36] J. Gong, D.W. Flaherty, R.A. Ojifinni, J.M. White, C.B. Mullins, J. Phys. Chem. C 112 (2008) 5501–5509.